STRESS ANALYSIS OF COATED PARTICLE FUEL IN GRAPHITE OF HIGH-TEMPERATURE REACTORS

FUEL CYCLE AND MANAGEMENT

KEYWORDS: *high-temperature reactors, stress analysis, coated particle fuel*

B. BOER* *Delft University of Technology, Mekelweg 15, 2629 JB Delft The Netherlands*

A. M. OUGOUAG *Idaho National Laboratory, 2525 N. Fremont Avenue Idaho Falls, Idaho*

J. L. KLOOSTERMAN *Delft University of Technology, Mekelweg 15 2629 JB Delft, The Netherlands*

G. K. MILLER *Idaho National Laboratory, 2525 N. Fremont Avenue Idaho Falls, Idaho*

Received June 24, 2007
Accepted for Publication November 1, 2007

The PArticle STress Analysis (PASTA) code was written to evaluate stresses in coated particle fuel embedded in graphite of high-temperature reactors (HTRs). Existing models for predicting stresses in coated particle fuels were extended with a treatment of stresses induced by dimensional change of the matrix graphite and stresses caused by neighboring particles.

PASTA was applied to two practical cases in order to evaluate the significance of this model extension. Thermal hydraulics, neutronics, and fuel depletion calculation tools were used to calculate the fuel conditions in these cases. Stresses in the first fuel loading of the High-Temperature Engineering Test Reactor (HTTR) and in the fuel of a 400-MW(thermal) pebble bed reactor were analyzed.

It is found that the presence of the matrix material plays a significant role in the determination of the stresses that apply to a single isolated TRISO particle as well as in the transmittal of the stresses between particles in actual pebble designs.

I. INTRODUCTION

The fuel design for nearly all high-temperature reactors (HTRs) currently planned and investigated is largely based on experience gained primarily in German research reactors[1] during several decades (AVR, THTR, Dragon designs, etc.). These designs of the pebble bed type contain several hundreds of thousands of pebbles that form a porous bed, which is cooled with helium gas. The graphite pebbles, with a diameter of 6 cm, contain the nuclear fuel within their fueled region of 5-cm radius. This fueled region consists of a graphite matrix containing tens of thousands of TRISO-coated particles. The TRISO particles have a UO_2 (or UC) kernel at their very center. Adjacent to the kernel is a porous carbon buffer layer, which is coated with an inner pyrolytic carbon (IPyC) layer, a silicon carbide (SiC) layer, and an outer pyrolytic carbon (OPyC) layer. These coatings provide the primary containment of the fission products that are generated in the fuel kernel. As a consequence, numerous publications on integrity and performance of the TRISO-coated particle can be found in the literature since the 1960s (Ref. 2), ranging from stress analysis investigations[3] to recent fully integrated fuel performance models.[4–9]

Trends in the intended operating conditions of the very-high-temperature reactor[10] (VHTR), such as higher fuel temperatures and higher discharge burnup values, call for a reconsideration of these earlier fuel and reactor designs. Of particular interest are the stresses in the

*E-mail: b.boer@tudelft.nl

particle coatings and the corresponding particle failure probability, which is expected to increase under the contemplated new operating conditions.

TRISO particles in HTRs experience stresses due to fission product buildup within the buffer layer, shrinkage/swelling of the pyrocarbon layers, and thermal expansion of all the layers during transients. In most analyses of stresses and strains, the mechanical model consists of a single particle in vacuum.[3,5] However, in the fuel zone of today's pebble designs, the TRISO particles can be within a short distance of one another,[11] and it is therefore likely that the stress fields of neighboring particles influence the stress state of a given particle. Furthermore, the graphite in which the particles are embedded experiences dimensional change under irradiation, which in turn causes additional stresses on the fuel particles.

The PArticle STress Analysis (PASTA) code is developed to calculate the stresses in the different layers of the coated particles and surrounding graphite during irradiation. This code is an extension of existing analytical models,[3] based on viscoelastic description of stresses, and is able to quantify the abovementioned effects.

In Sec. II a detailed derivation of this analytical model is presented. Section III presents the theory of the stress effects caused by the dimensional changes of the matrix graphite and neighboring particles. In Sec. V the stress analysis code is applied to two cases in order to quantify the above effects in particle fuel of present-day reactor designs, namely, (the first fuel loading of) the High-Temperature Engineering Test Reactor[12] (HTTR) and a 400-MW(thermal) pebble bed reactor design. Prior to the use of PASTA for the various designs, additional calculations have to be performed in order to supply the code with realistic boundary conditions. The calculation procedure that is used to determine the particle conditions (i.e., internal pressure, dimensional changes, and fluence) is presented in Sec. IV. Limitations of the code and possible future work are discussed in Sec. VI.

II. DERIVATION OF AN ANALYTICAL MODEL FOR A FOUR-LAYER PRESSURE VESSEL

An analytical model is set up to calculate the tangential stress as a function of the (fast) neutron dose in the coatings of the fuel particle and the surrounding graphite matrix. The approach taken is based on previously developed models.[3,13] The major difference between those models and the current work is the addition of an extra layer representing the graphite matrix material surrounding the TRISO particle (see Fig. 1). By including this layer the effect of the graphite matrix dimensional changes and the stress effect of neighboring particles can be modeled. It is noted that as in the existing models, the fuel kernel and buffer layer are not explicitly represented. It is assumed that possible swelling of the fuel kernel can be accommodated by the surrounding porous buffer layer.

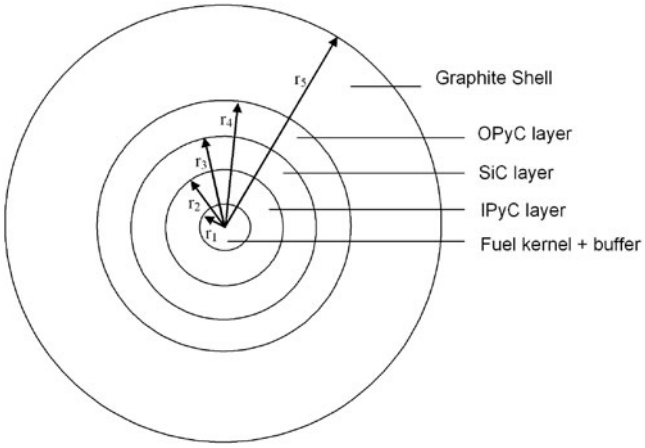

Fig. 1. Geometry of a TRISO particle and graphite layer.

In Sec. II.A the equations for the stresses in a four-layer pressure vessel are derived. The creep behavior in the pyrocarbon layers of the fuel particle and in the graphite matrix are modeled using a Maxwellian creep model. This model assumes that the steady-state strain rate can be represented by an elastic model (spring) and a viscous model (dash pot) in series.[13] Transient creep is ignored because effects are expected to be small.[14]

II.A. Governing Equations and Solution

The strain derivatives with respect to the neutron fluence t for the radial and tangential directions in a spherical element, including the source terms for the irradiation dimensional change rate ($\dot{S}_r$ and $\dot{S}_t$) and the thermal expansion rates ($\alpha_r \dot{T}$ and $\alpha_t \dot{T}$), can be written as (see Nomenclature on p. 290)

$$\frac{\partial \varepsilon_r}{\partial t} = \frac{1}{E}\left[\frac{\partial \sigma_r}{\partial t} - 2\mu \frac{\partial \sigma_t}{\partial t}\right] + c[\sigma_r - 2\nu\sigma_t] + \alpha_r \dot{T} + \dot{S}_r \qquad (1)$$

and

$$\frac{\partial \varepsilon_t}{\partial t} = \frac{1}{E}\left[(1-\mu)\frac{\partial \sigma_t}{\partial t} - \mu \frac{\partial \sigma_r}{\partial t}\right] + c[(1-\nu)\sigma_t - \nu\sigma_r] + \alpha_t \dot{T} + \dot{S}_t \ . \qquad (2)$$

From the strain-displacement relations and equilibrium requirement follows[15]

$$\varepsilon_r = \frac{\partial u}{\partial r} \ , \qquad (3)$$

$$\varepsilon_t = \frac{u}{r} \ , \qquad (4)$$

and

$$\frac{\partial \sigma_r}{\partial r} + \frac{2}{r}(\sigma_r - \sigma_t) = 0 \ , \tag{5}$$

where u is the radial displacement.

In order to find the solutions to Eqs. (1) through (5), the same procedure is used as in Ref. 16. The closed form solution in Ref. 16 is an improvement over the earlier solution found in Ref. 13 and allows the material properties to change with irradiation time (or dose). Furthermore, the solution allows for the Poisson's ratio of creep to deviate from $\nu = 0.5$.

The solutions for the radial displacement and for the radial and tangential stresses are assumed to be in form of series[3]:

$$u(r,t) = \sum_{i,n=0}^{\infty} u_i t^n \ , \tag{6}$$

$$\sigma_r(r,t) = \sum_{i,n=0}^{\infty} \sigma_{r,i} t^n \ , \tag{7}$$

and

$$\sigma_t(r,t) = \sum_{i,n=0}^{\infty} \sigma_{t,i} t^n \ . \tag{8}$$

The incremental solution for the displacement can be found by combining Eqs. (1) through (8) (Ref. 3):

$$\frac{d^2 u_i}{dr^2} + \frac{2du_i}{rdr} - \frac{2}{r^2} u_i = \frac{2}{Er}(1-2\mu) f_i + \frac{2}{r} c(1-2\nu)\frac{f_{i-1}}{i} \tag{9}$$

and

$$f_{i+1} = -\frac{cE(1-\nu)}{(1-\mu)}\frac{f_i}{i+1} + \frac{E(\dot{S}_{r,i} - \dot{S}_{t,i} + \alpha_r \dot{T}_i - \alpha_t \dot{T}_i)}{(1-\mu)(i+1)} \ , \tag{10}$$

where $f_0 = 0$.

A function $F(t)$ can be defined by

$$F(t) = \sum_{i,n=1}^{\infty} f_i t^n \ . \tag{11}$$

This function is used later in this paper to determine the stresses within the coating layers.

The incremental solution for the displacement obtained from Eqs. (9) and (10) is

$$u_i = A_i r + \frac{B_i}{r^2} + \left[\frac{2(1-2\mu)}{3E} f_i + \frac{2c(1-2\nu)}{3i} f_{i-1}\right] r \ln(r) \ . \tag{12}$$

Using Eq. (12), the corresponding equations for the incremental stresses can be found:

$$\begin{aligned}\sigma_{r,i} = {} & \frac{E}{(1-2\mu)} A_i - \frac{E}{(1+\mu)}\frac{2B_i}{r^3} \\ & + \frac{2}{3}((1+\mu)\ln(r) + (1-\mu))\left[\frac{1}{(1+\mu)} f_i + \frac{Ec(1-2\nu)}{(1+\mu)(1-2\mu)i} f_{i-1}\right] \\ & - \frac{cE}{(1+\mu)i}\left[\left(1 + \frac{\mu(1-2\nu)}{(1-2\mu)}\right)\sigma_{r,i-1} + \left(\frac{(1-2\nu)}{(1-2\mu)} - 1\right)\sigma_{t,i-1}\right] \\ & - \frac{E(2\mu(\dot{S}_{t,i-1} + \alpha_t \dot{T}_{i-1}) + (1-\mu)(\dot{S}_{r,i-1} + \alpha_r \dot{T}_{i-1}))}{(1+\mu)(1-2\mu)i}\end{aligned} \tag{13}$$

and

$$\begin{aligned}\sigma_{t,i} - \sigma_{r,i} = {} & \frac{3E}{(1+\mu)}\frac{B_i}{r^3} - \frac{2}{3(1+\mu)}\left[(1-2\mu) f_i + \frac{Ec(1-2\nu)}{i} f_{i-1}\right] \\ & + \frac{Ec(1+\nu)}{(1+\mu)i}(\sigma_{r,i-1} - \sigma_{t,i-1}) + \frac{E((\dot{S}_{r,i-1} + \alpha_r \dot{T}_{i-1}) - (\dot{S}_{t,i-1} + \alpha_t \dot{T}_{i-1}))}{(1+\mu)i} \ .\end{aligned} \tag{14}$$

The internal and external pressures $p(t)$ and $q(t)$ are applied as the boundary conditions at the inner and outer radii of the layer under consideration, i.e., at r_a and r_b, respectively, by expressing them in the following forms:

$$p(t) = \sum_{i,n=0}^{\infty} p_i t^n$$

and

$$q(t) = \sum_{i,n=0}^{\infty} q_i t^n \quad . \tag{15}$$

In this sign convention the pressures $p(t)$ and $q(t)$ are positive outward. Following Ref. 13, Eq. (13) is used to equate the radial stress at the surfaces to the above pressures. The coefficients A_i and B_i can now be found. Furthermore, a useful relation that applies for the radial and tangential stress components in a spherical shell, between radii r_a and r_b, is derived from Eq. (14):

$$\sigma_{t,i}(r) - \sigma_{r,i}(r) = \frac{3(r_a r_b)^3}{r^3(r_a^3 - r_b^3)}\left(p_i - q_i - \frac{2}{3} f_i \ln\frac{r_a}{r_b}\right) + \frac{f_i}{3} \quad . \tag{16}$$

Equations (12) and (16) are combined, and a general expression for the displacement in a spherical layer is found:

$$u(r,t) = K_1 p(t) + K_2 q(t) + K_3 \int p(t) c\, dt + K_4 \int q(t) c\, dt + K_5 \int (\dot{S}_r(t) + \alpha_r \dot{T}(t))\, dt + K_6 \int (\dot{S}_t(t) + \alpha_t \dot{T}(t))\, dt + K_7 F(t) \quad . \tag{17}$$

The constants K_i are given in the Appendix and depend on the geometry and material properties of the layer. It is noted that the coefficient K_7 vanishes at the boundary interfaces.

Solutions for the displacement of each layer interface at any point in time are sought. The boundary conditions at each layer interface imply continuity of radial stress and displacement. The pyrocarbon and graphite layers are assumed to exhibit creep and anisotropic swelling, and all four layers are allowed to exhibit anisotropic thermal expansion. For all the layers the displacements at interfaces (i.e., layer inner and outer surfaces) are given by

IPyC outer surface:

$$u_I = a_1 p + a_2 \sigma_{r,I} + a_3 \int p c_I\, dt + a_4 \int \sigma_{r,I} c_I\, dt + a_5 \int (\dot{S}_{r,I} + \alpha_{r,I} \dot{T}_I)\, dt + a_6 \int (\dot{S}_{t_I} + \alpha_{t,I} \dot{T}_I)\, dt \quad ; \tag{18}$$

SiC inner and outer surfaces:

$$u_I = b_1 \sigma_{r,I} + b_2 \sigma_{r,O} + b_3 \int \alpha_{r,S} \dot{T}_S\, dt + b_4 \int \alpha_{t,S} \dot{T}_S\, dt \tag{19}$$

$$u_O = c_1 \sigma_{r,I} + c_2 \sigma_{r,O} + c_3 \int \alpha_{r,S} \dot{T}_S\, dt + c_4 \int \alpha_{t,S} \dot{T}_S\, dt \quad ; \tag{20}$$

OPyC inner and outer surfaces:

$$u_O = d_1 \sigma_{r,O} + d_2 \sigma_{r,X} + d_3 \int \sigma_{r,O} c_O\, dt + d_4 \int \sigma_{r,X} c_O\, dt + d_5 \int (\dot{S}_{r,O} + \alpha_{r,O} \dot{T}_O)\, dt + d_6 \int (\dot{S}_{t_O} + \alpha_{t,O} \dot{T}_O)\, dt \tag{21}$$

$$u_X = e_1 \sigma_{r,O} + e_2 \sigma_{r,X} + e_3 \int \sigma_{r,O} c_O\, dt + e_4 \int \sigma_{r,X} c_O\, dt + e_5 \int (\dot{S}_{r,O} + \alpha_{r,O} \dot{T}_O)\, dt + e_6 \int (\dot{S}_{t_O} + \alpha_{t,O} \dot{T}_O)\, dt \quad ; \tag{22}$$

Graphite-matrix:

$$u_X = f_1 \sigma_{r,X} + f_2 q + f_3 \int \sigma_{r,X} c_X\, dt + f_4 \int q c_X\, dt + f_5 \int (\dot{S}_{r,X} + \alpha_{r,X} \dot{T}_X)\, dt + f_6 \int (\dot{S}_{t_X} + \alpha_{t,X} \dot{T}_X)\, dt \quad , \tag{23}$$

where

p = pressure in the buffer layer

$\sigma_{r,I}$ = radial stress at the IPyC outer surface (or SiC inner surface due to continuity of radial stress through an interface)

$\sigma_{r,O}$ = radial stress at the OPyC inner surface

$\sigma_{r,X}$ = radial stress at the matrix graphite inner surface

q = pressure on the outer surface.

The coefficients $a_i, b_i, \ldots, f_i$ can be calculated from the constants K_i given in the Appendix by inserting the appropriate values for the layers.

II.B. Radial Stresses at the Interfaces

Equations (18) through (23) are combined to obtain a system of equations for the radial stress at the interfaces. For the above four-layer problem, a system of three inhomogeneous linear equations is obtained:

$$\dot{\boldsymbol{\sigma}}_r - \boldsymbol{B}\boldsymbol{\sigma}_r = \boldsymbol{G}(t) \ , \tag{24}$$

which has the solution[17]

$$\boldsymbol{\sigma}_r = \sum_{i=1}^{3} C_i \boldsymbol{\xi}_i e^{\lambda_i t} + \boldsymbol{g}_0 + \boldsymbol{g}_1 t \ , \tag{25}$$

where

$\boldsymbol{\xi}_i$ = eigenvectors of the system

λ_i = eigenvalues of the system

C_i = constants determined by the initial conditions.

In practice the eigenvalues and eigenvectors can be quickly calculated by numerical procedures. After this computation step the vectors $\boldsymbol{g}_0$ and $\boldsymbol{g}_1$ are calculated by inserting Eq. (25) into Eq. (24) and performing a simple Gauss elimination.

II.C. The Function $F(t)$

When the radial stresses at the layer interfaces are known, the radial and tangential stresses at each point within the layers can be determined. Substituting Eq. (10) into Eq. (11) and differentiating with respect to t yields Eq. (26) for the function F:

$$\frac{dF}{dt} + \frac{cE(1-\nu)}{1-\mu} F = \frac{E}{1-\mu} \left(\overline{\dot{S}_r} + \overline{\alpha_r \dot{T}} - \overline{\dot{S}_t} - \overline{\alpha_t \dot{T}}\right) \ , \tag{26}$$

where the overline indicates that the relevant property is averaged over the time interval. The general solution for the function $F(t_n)$ is obtained by integrating between t_{n-1} and t_n:

$$F(t_n) = [F(t_{n-1}) - \gamma_0] e^{-\beta(t_n - t_{n-1})} + \gamma_0 \ , \tag{27}$$

where

$$\beta = \frac{cE(1-\nu)}{(1-\mu)} \tag{28}$$

and

$$\gamma_0 = \frac{\overline{\dot{S}_r} - \overline{\dot{S}_t} + \overline{\alpha_r \dot{T}} - \overline{\alpha_t \dot{T}}}{c(1-\nu)} \ . \tag{29}$$

II.D. General Stress Equations

Equation (25) gives the radial contact stresses at the interface of the layers. Together with Eq. (27) it is possible to determine radial and tangential stresses at any position in the layers following the procedure in Ref. 13. This results in Eqs. (30) and (31):

$$\sigma_r(r,t) = \frac{r_a^3(r_b^3 - r^3)}{r^3(r_b^3 - r_a^3)} p - \frac{r_b^3(r_a^3 - r^3)}{r^3(r_b^3 - r_a^3)} q - \frac{2}{3}\left[\frac{r_a^3(r_b^3 - r^3)\ln r_a - r_b^3(r_a^3 - r^3)\ln r_b}{r^3(r_b^3 - r_a^3)} - \ln r\right] F(t) \tag{30}$$

and

$$\sigma_t(r,t) = -\frac{r_a^3(r_b^3 + 2r^3)}{2r^3(r_b^3 - r_a^3)} p + \frac{r_b^3(r_a^3 + 2r^3)}{2r^3(r_b^3 - r_a^3)} q + \frac{1}{3}\left[\frac{r_a^3(r_b^3 + 2r^3)\ln r_a - r_b^3(r_a^3 + 2r^3)\ln r_b}{r^3(r_b^3 - r_a^3)} + 2\ln r + 1\right] F(t) \ . \tag{31}$$

III. STRESS EFFECTS IN THE GRAPHITE MATRIX

III.A. Stress Effects due to Dimensional Change of the Graphite Matrix

The four-layer model that was derived in Sec. II is now used to investigate the effects of adding a graphite layer to the three-layer model. It is noted that at first the irradiation-induced dimensional change of the fourth (graphite) layer is not taken into account. The properties of the particle and the graphite that were used for the calculations are shown in Table I. The thickness of the graphite layer is chosen in such a way that its volume is equivalent to the average graphite volume per particle. For a pebble with 15 000 fuel particles and an outer radius of the OPyC of $r_4 = 0.0465$ cm, the graphite equivalent layer thickness is 0.058 cm and $r_5 = 0.105$ cm.

TABLE I

Values Used for Evaluating Effect of Graphite Dimensional Change

Item	Value
Kernel diameter (μm)	500
Buffer thickness (μm)	95
IPyC thickness (μm)	40
SiC thickness (μm)	35
OPyC thickness (μm)	40
Dimensional change of the PyC layers	Eqs. (36), (37)
Creep constant of PyC layers $[(\text{MPa}\cdot 10^{25}\ \text{m}^{-2})^{-1}]$	3.0×10^{-4}
Young's modulus of PyC (MPa)	3.96×10^{4}
Young's modulus of SiC (MPa)	4.0×10^{5}
Young's modulus of C matrix (MPa)	1.05×10^{4}

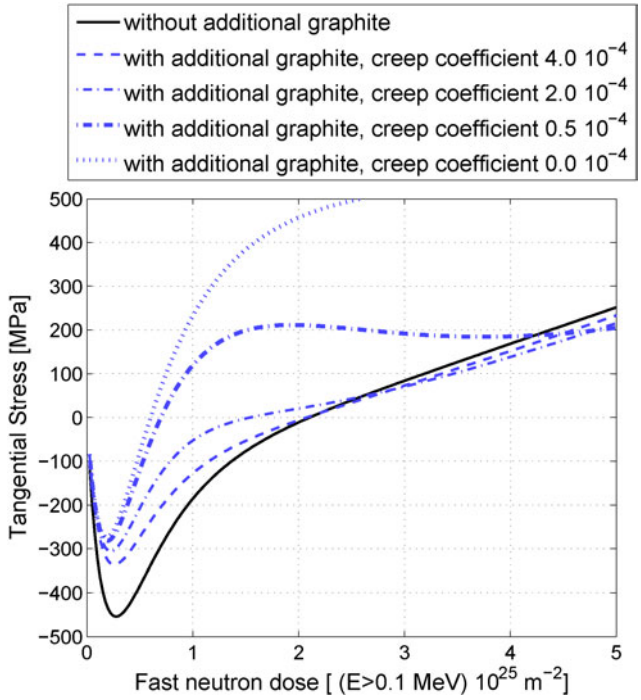

Fig. 2. Effect of the presence of graphite matrix on SiC tangential stress (excluding dimensional change of graphite). The continuous line represents the case without the additional graphite layer; the dashed/dotted lines represent the cases with a graphite layer for several values of the irradiation creep coefficient [in $(\text{MPa}\cdot 10^{25}\ \text{m}^{-2})^{-1}$].

Figure 2 shows that the presence of the graphite material has a significant effect on the tangential stress in the SiC layer. High tensile stresses are found in the early stage of the irradiation for cases in which the graphite has a low irradiation creep constant. Taking a high value for the creep constant reduces the tangential stress, and the corresponding solution tends to the solution for a particle without the additional graphite layer. In reality, the graphite matrix experiences irradiation-induced dimensional changes as well as thermal expansion.[18] Measurements on the dimensional change of graphite have been performed during operation of the AVR reactor[18] by measuring the pebble diameter. In Fig. 3 the dimensional change rate remains negative, while others have found that for some graphite material a turnaround exists beyond which the dimensional change rate becomes positive.[19]

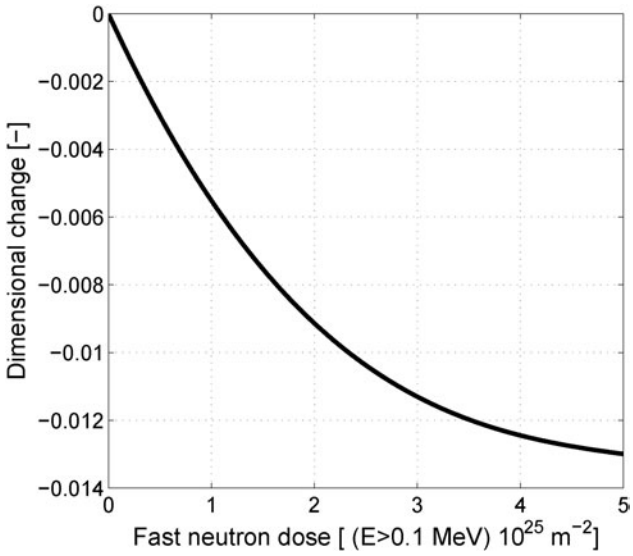

Fig. 3. Dimensional change of a pebble in the AVR, taken from Ref. 18.

The effect of the graphite matrix dimensional change on the SiC tangential stress is shown in Fig. 4, for which the result presented in Fig. 3 was implemented in the stress analysis model. The continuous line presents the case in which no dimensional change of the graphite matrix was assumed, while the dashed lines represent cases with dimensional change for various creep constants of the graphite matrix. Note that the creep constant of the pyrocarbon material is kept at a fixed value of $3.0 \times 10^{-29}\ (\text{MPa}\cdot\text{m}^{-2})^{-1}$.

It is concluded that for all cases the dimensional change rate of the graphite layer has a significant impact on the tangential stress of the SiC layer. The time at which the tangential stress becomes positive depends on the value of the creep coefficient of the graphite matrix. From Refs. 20 and 21 the irradiation creep coefficient for high-temperature gas-cooled reactor (HTGR) graphite was determined to be in the range of 3.4×10^{-29} to $4.8 \times 10^{-29}\ (\text{MPa}\cdot\text{m}^{-2})^{-1}$ (for $E > 0.18$ MeV) at 1029 to 1257 K, with an average value of $4.2 \times 10^{-29}\ (\text{MPa}\cdot\text{m}^{-2})^{-1}$. The latter is used in the following calculations.

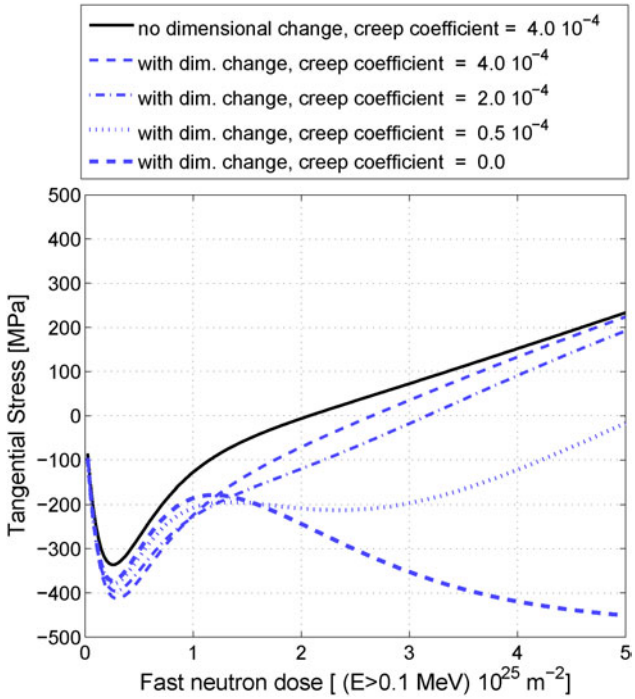

Fig. 4. Effect of graphite matrix dimensional change on SiC tangential stress, for several values of the irradiation creep coefficient [in $(\text{MPa}\cdot 10^{25}\ \text{m}^{-2})^{-1}$].

III.B. Interparticle Stress Effects

In most analyses of stresses and strains of fuel particles, the mechanical model consists of a single particle in vacuum. However, in the fueled zone of today's pebble designs, the TRISO particles are within a short distance from one another, and it is therefore likely that the stress field of a given particle will influence the stress state of its neighbors. The distance of the neighboring particles determines the magnitude of the stress that a given particle sees on its surface.

In practical cases the radial and tangential stress components differ in magnitude and sign (compression or tension). In Fig. 5 the position on a TRISO surface, determined with radius R and angles θ and φ, is denoted with P. At this position on the particle surface, radial and tangential stresses are present, resulting from the particle itself. The radial stress component has the direction of line OP. Furthermore, radial and tangential stresses coming from a neighboring particle, at a distance d, with its center at O′, are also acting on point P. The direction of the radial stress of the neighboring particle is along line O′P. It must be kept in mind that in practical cases the radius of the particle is of the same order of magnitude as the distance d, for the closest neighbors. The magnitude of the radial and tangential stress components can be calculated with Eqs. (30) and (31), respectively, in which r is equal to O′P.

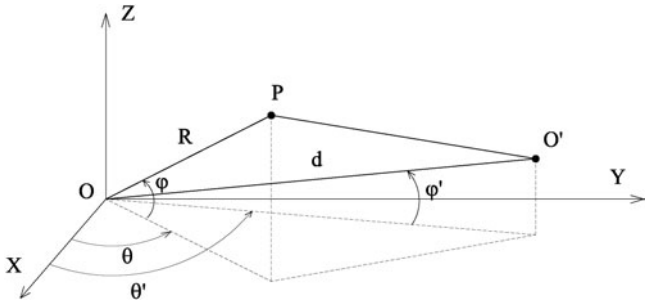

Fig. 5. Orientation of a TRISO particle at O and its neighbor at O′.

In order to calculate the total stress field, the stress components ($\boldsymbol{\sigma}'$) from the neighbor can be transformed to a stress tensor in the coordinate system of the given particle ($\boldsymbol{\sigma}$), with

$$\boldsymbol{\sigma} = \boldsymbol{L}\boldsymbol{\sigma}'\boldsymbol{L}^T \ , \qquad (32)$$

in which $\boldsymbol{L}$ is the transformation matrix, consisting of the direction cosines between the two coordinate systems.[15,22]

This procedure is applied to several neighboring particles, assuming that all neighbors have the same stress state and that the stresses can be superimposed. Because the creep strain derivative depends on the actual stress itself, the creep effect leads to nonlinear behavior of the stress in time [see Eqs. (1) and (2)]. Therefore, the actual combined stress from multiparticle effects should result in slightly more creep strain (and consequently more stress relief in the graphite) than will be calculated from summing individual particle stresses.

From Eqs. (30) and (31), it can be seen that the magnitude of the stress reduces with one over the distance cubed. However, the number of neighboring particles at a given distance increases with the distance squared. Therefore, neighbors that are within considerable distance of the particle considered have to be taken into account.

For the sake of model development, it is first considered that the particles are distributed regularly in the matrix material. Figure 6 shows a cubic distribution of particles, but a hexagonal and a random distribution are also considered in this paper. The combined maximum principal stress resulting from all neighbors within a certain distance is presented in Fig. 7 for a cubic distribution of the neighbors.

The interparticle stress effect is determined by calculating the principal stresses for several points on the surface of the particle. In Fig. 7 the maximum principal stress is presented as a function of the distance from the particle. With increasing distance, the number of neighbors to be taken into account increases, assuming that the particle considered is at the center of the pebble. At a

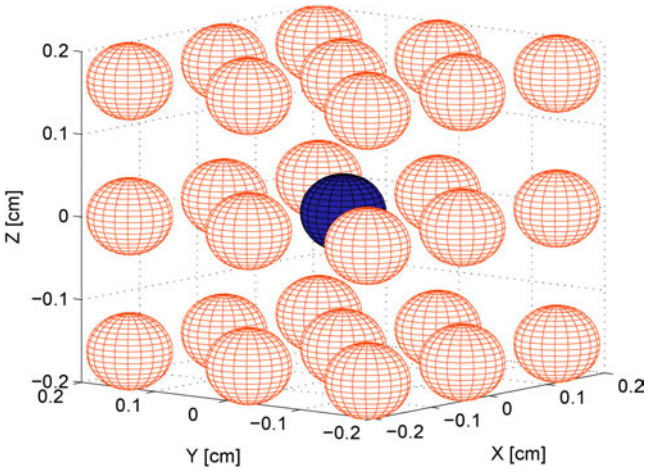

Fig. 6. Position of neighboring fuel particles (light) with regard to a given particle (dark) for a cubic lattice.

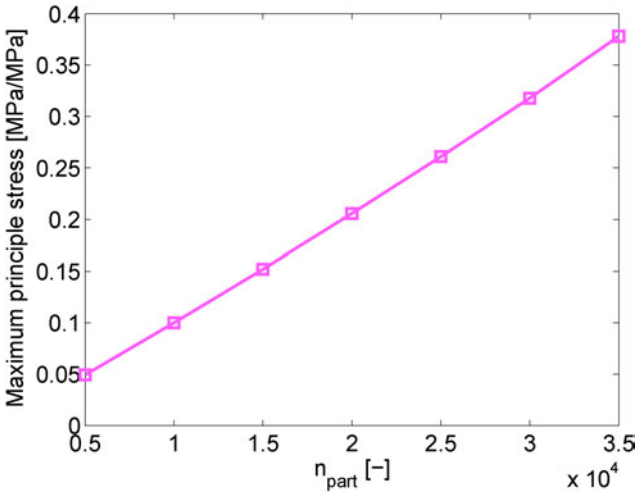

Fig. 8. Maximum principal stress dependent on the number of particles in a pebble.

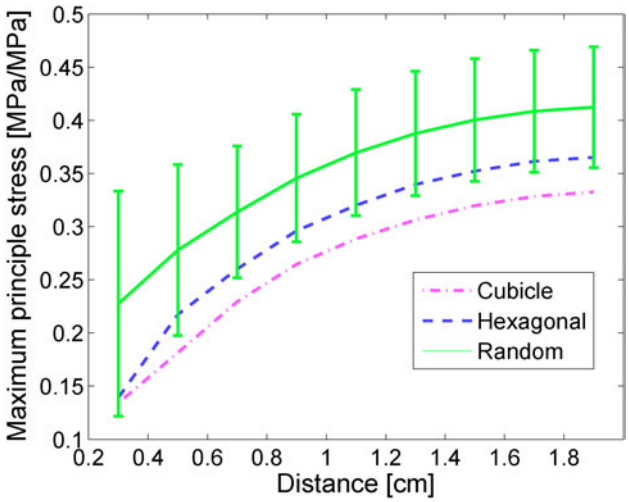

Fig. 7. Maximum principal stress normalized to a radial stress of 1 MPa at the surface of the TRISO particles, resulting from neighbors within the specified distance from the particle.

large distance the stress effect from the neighbors becomes small. However, the distance from which the contribution to the total stress effect can be neglected is relatively large with regard to the particle diameter. On the other hand, a large part of the effect is determined by the closest neighbors. This can also be concluded from the stress effect for randomly distributed neighbors. The standard deviation from the average stress effect is also presented in Fig. 7 and shows a large spread, especially for short distances. In the random distribution, a neighbor can be a short distance from the particle, which results in a large effect on the stress. This can explain why the random distribution gives the highest interparticle stress effect, resulting in an increase of 40% of the radial stress at the surface of the particle.

The above calculations were performed for a pebble containing 15 000 TRISO particles. Figure 8 shows the dependency of the relative maximum principal stress on the number of particles contained in the pebble (for a cubic distribution, considering neighbors within a distance of 0.3 cm). One can see that the stress effect has a quasi-linear dependency on the particle packing fraction.

III.B.1. Conclusion on Interparticle Stress

In the above analysis it is found that the interparticle stress effect is ~40% of the radial stress at the outer surface of a particle for a pebble containing 15 000 randomly distributed TRISO particles. Figure 9 shows the radial stress at the surface of a single particle during irradiation, calculated with the four-layer model and assuming the same conditions as in Sec. III.A (excluding the effect of the graphite matrix dimensional change).

To quantify the interparticle effect, the radial stress presented in Fig. 9 is used in a three-layer model as a boundary condition to calculate the effect on the maximum tangential stress in the SiC layer. The radial stress at the surface is therefore increased by a factor between 1 and 2, to represent the stress effects of the neighboring particles. It must be noted that this is a first approximation of the interparticle stress effect. In reality the stress field on the surface of the particle, resulting from neighboring particles, will not exactly be radially uniform.

The results of the calculations are shown in Fig. 10. It can be seen that there is a small effect on the SiC tangential stress for the case of 40% stress increase (factor 1.4), especially at the beginning of the irradiation. In general the tangential stress is reduced for this irradiation case, being either less compressive or less tensile.

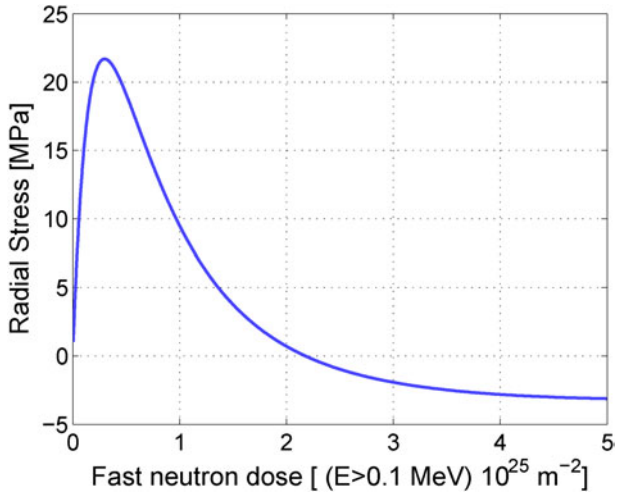

Fig. 9. Radial stress at the outer surface of the OPyC layer of a TRISO particle during irradiation.

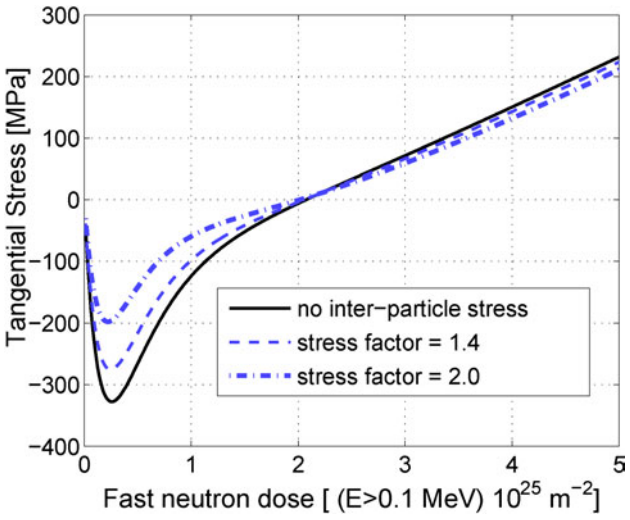

Fig. 10. Tangential stress of the SiC layer for several values of radial stress increase acting on the outer surface of the particle.

IV. CALCULATION PROCEDURE IN STRESS ANALYSIS

Prior to the use of the stress analysis code PASTA, input data such as the internal pressure on the IPyC layer dependent on neutron fluence and the dimensional changes of the layers have to be known. A schematic overview of the calculation procedure that is used to find these data is given in Fig. 11. This procedure is adopted in the stress analyses of Sec. V.

First, the neutron flux, burnup, and temperature profiles of the reactor core are calculated with existing codes and methods. These data are exploited to calculate the gaseous fission product generation inside the kernel, and their diffusion to and build up within the buffer layer. Also computed is the shrinkage/swelling of the pyrocarbon layers during the lifetime of the particle. During each time step, corresponding to a certain position of the pebble in the core and a certain irradiation dose, the mechanical stresses are evaluated. Sections IV.A through IV.D provide a more detailed description of the different calculation tools and assumptions that are used in this context.

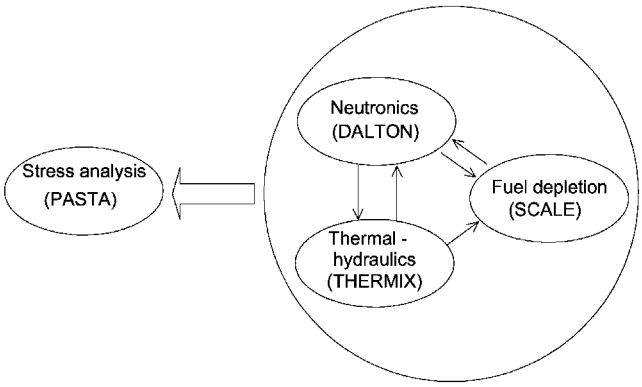

Fig. 11. Code system overview.

IV.A. Neutronics and Thermal Hydraulics

As shown in Fig. 11, the neutronics code DALTON is used to calculate the neutron flux and power profile. DALTON is able to perform three-dimensional calculations for eigenvalue and transient neutron diffusion problems using a finite difference scheme and has been used before in HTR neutronic calculations.[23]

In the stress analysis of Sec. V.B, a two-dimensional (2-D) cylindrical geometry with axial symmetry is used to model the neutronics of the reactor. The power profile is passed to the thermal-hydraulics code, while the flux profile is radially collapsed to a one-dimensional (1-D) axial profile and supplied to the fuel depletion calculation.

The thermal-hydraulics code THERMIX (Direkt)[24] is used to compute the temperature profile from the given power profile. By performing iterative coupled calculations with the neutronics–thermal-hydraulics codes, the steady-state operating conditions of the design are determined.

To calculate the temperatures in the fuel particles, the results of THERMIX are used in an additional calculation,[25] which takes into account the thermal resistance of a possible gap between the porous buffer layer and the inner pyrocarbon layer.

IV.B. Fuel Depletion Calculation and Neutron Cross-Section Generation

In order to provide information on the fuel burnup level during irradiation, a nuclide depletion calculation,

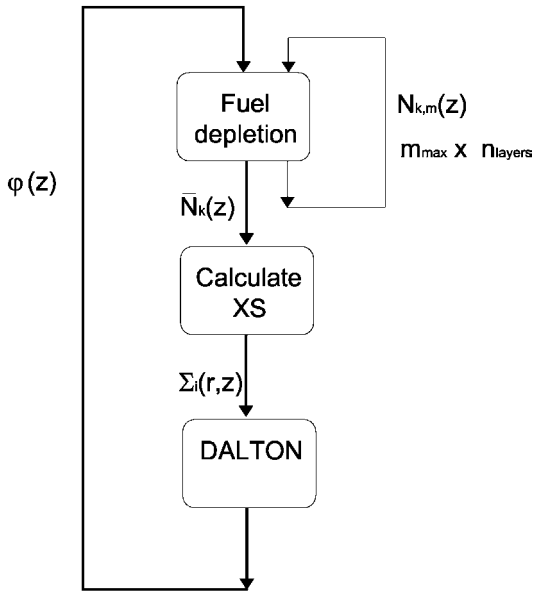

Fig. 12. Scheme of fuel depletion calculation (XS = cross section).

using several modules of the SCALE-5 code system,[26] is performed. To fix the neutron flux profile, it is assumed that the nuclide concentrations are in equilibrium. From this point, the burnup calculation procedure is as follows (as shown in Fig. 12).

Burnup calculation—For each axial layer z in the core and for each pass m through the core, the nuclide concentrations in the pebble are updated by using an axial flux profile computed by DALTON. Each axial layer in the core contains an equal number of k pebbles of different burnup states. The number of different burnup states per layer is equal to the number of passes $m_{\max}$. The total number of pebbles with different burnup states equals the number of passes ($m_{\max}$) times the number of axial layers (n_{layers}). For each layer n in the core, the nuclide concentrations are averaged, resulting in an axially averaged nuclide concentration $\bar{N}_k$.

Calculation of cross section—The nuclide concentrations are then used for generating neutron cross sections for the whole reactor geometry. The double heterogeneity of the fuel is taken into account by performing a cell weighting of a fuel particle in moderator material using an appropriate Dancoff factor[27] followed by a 1-D transport calculation of a pebble geometry. One-dimensional radial and axial transport calculations are used to calculate zone weighted cross sections for the entire reactor.

DALTON—The neutron cross sections are used to calculate the 2-D flux profile with the diffusion code DALTON. This profile is radially averaged to provide the burnup calculation with an axial flux profile.

The calculation steps are repeated until convergence is reached for the final discharge burnup and neutron flux profile.

IV.C. Irradiation Effects in the Particle Coatings During Operation

The gaseous fission products accumulate during irradiation in the buffer layer and induce a pressure buildup that depends on the kernel temperature and buffer volume.

IV.C.1. Formation and Diffusion of Gaseous Fission Products in the Fuel Kernel

The buildup of gaseous fission products can be calculated analytically and numerically[5,28] by solving the time-dependent fission product diffusion equation

$$\frac{\partial C}{\partial t} = \frac{D}{r^2}\frac{\partial}{\partial r}\left(r^2\frac{\partial C}{\partial r}\right) + Q \ , \qquad (33)$$

where

C = fission product concentration (cm^{-3})

r = radial position in the kernel (cm)

D = diffusion coefficient ($\mathrm{cm}^2\cdot\mathrm{s}^{-1}$)

Q = source term of fission products ($\mathrm{cm}^{-3}\cdot\mathrm{s}^{-1}$).

The source term is determined by the local power in the reactor. It is assumed that 31% of the fission products are gaseous krypton and xenon.[29] The numerical approach is preferred and used to solve Eq. (33). This method allows for a nonzero concentration at the boundary, which is an improvement compared to the analytical approach in which a zero concentration in the porous buffer layer is usually assumed throughout the irradiation period.[28]

Besides direct formation of gaseous fission products, formation of CO gas by a reaction of the oxygen present in the fuel kernel and carbon in the buffer layer is possible. The formation of this gas is taken into account by the following empirical formula[29,30] for oxygen release per fission:

$$O/f = 8.32\cdot10^{-11}t_{irr}^2 e^{(-Z/R\cdot T)} \ , \qquad (34)$$

where

O/f = number of oxygen atoms released per fission, after an irradiation time t_{irr} (s)

Z = 162.7 $\mathrm{kJ}\cdot\mathrm{mol}^{-1}$

R = universal gas constant ($\mathrm{J}\cdot\mathrm{mol}^{-1}\cdot\mathrm{K}^{-1}$)

T = temperature (K).

IV.C.2. Calculation of the Pressure in the Buffer Layer

The resulting pressure on the IPyC layer is calculated with the Redlich Kwong equation of state[31] as a function of the kernel temperature and the buffer volume:

$$RT_{kernel} = \left(P + \frac{a}{T_{kernel}^{1/2} V_m (V_m + b)} \right) (V_m - b) \quad . \quad (35)$$

The ideal gas law is not applied here because it underpredicts the pressure significantly.[6]

IV.C.3. Dimensional Change and Creep of Particle Coatings

Under irradiation, the PyC layers are exposed to a fast neutron flux, which causes dimensional changes. The dimensional change rate is dependent on the initial density and anisotropy of the pyrocarbon material. Several empirical relations for the radial and tangential dimensional change rate exist.[6] In general the layers shrink at low neutron dose. This shrinking eventually comes to a halt at higher irradiation dose. In some cases, depending on the material properties, the shrinking turns into swelling at higher doses. The following relations recommended by the Forschungszentrum Jülich in Germany are adopted in the present fuel performance model[6]:

$$\dot{S}_r = -0.077 e^{(-t)} + 0.031 \quad (36)$$

and

$$\dot{S}_t = -0.036 e^{(-2.1t)} - 0.01 \quad , \quad (37)$$

where

$\dot{S}_r, \dot{S}_t$ = dimensional change rates in the radial and tangential directions, respectively, expressed in $(10^{25}\ \mathrm{m}^{-2})^{-1}$

t = fast neutron fluence (for energies $E > 0.1$ MeV) expressed in $10^{25}\ \mathrm{m}^{-2}$.

Moreover, pyrocarbon and graphite materials creep under irradiation, partly reducing the stress. For the pyrocarbon layers a value of 3.0 $(\mathrm{MPa}\cdot 10^{21}\ \mathrm{m}^{-2})^{-1}$ is taken for the creep coefficient from literature[6] and a value of 4.2 $(\mathrm{MPa}\cdot 10^{21}\ \mathrm{m}^{-2})^{-1}$ for the matrix graphite is adopted from Refs. 20 and 21.

IV.D. Calculation of the Failure Fraction of SiC

The combined effects of the fission product buildup in the buffer, the dimensional change, and the creep of the PyC layers lead to a certain stress in the SiC layer. The SiC layer is the main load bearer within the TRISO particle and can withstand high compressive stresses, but it can fail under high tensile stresses. The failure fraction of the SiC layer in the kernel can be calculated using the Weibull distribution function[6,12,32]

$$\Phi = 1 - e^{-\ln 2 (\sigma_t / \sigma_{med})^m} \quad , \quad (38)$$

where

σ_t, σ_{med} = maximum tangential (tensile) stress and the median strength in the SiC, respectively

m = modulus, taken to be 8.0

and the median strength is taken as 834 MPa, as reported in Ref. 12.

V. APPLICATION AND RESULTS

In order to quantify the effect of the extra graphite layer in the stress analysis code PASTA, two applications of PASTA to present-day HTR fuel designs are carried out. The first application is the first fuel loading of the HTTR, and the second application is a 400-MW(thermal) HTR design.

V.A. Stress Analysis of the First Fuel Loading of the HTTR

PASTA is applied to the irradiation experiment of the first fuel loading of the HTTR (Ref. 12). A stress analysis calculation was also performed by Sawa et al.[12] and with the TIMCOAT code.[5] For dimensional change rates of the PyC layers, Eqs. (36) and (37) were used. The data used for this calculation are presented in Table II. Cases with and without the effects of the dimensional change of the graphite matrix and interparticle stress are considered.

Figure 13 shows that the results for the tangential stress in the SiC layer obtained with the PASTA code are in good agreement with the other two codes. At the

TABLE II

Properties of Particle Fuel in HTTR Irradiation Experiment

Item	Value
Fuel density $(\mathrm{g}\cdot\mathrm{cm}^{-3})$	10.7
Enrichment (%)	9.17
Kernel diameter (μm)	600
Buffer thickness (μm)	60
IPyC thickness (μm)	30
SiC thickness (μm)	25
OPyC thickness (μm)	45
Fuel temperature (K)	1573
End-of-life fast fluence (m^{-2})	3.0×10^{25}
End-of-life burnup (GWd/t)	66
Irradiation time (day)	100
PyC creep constant $(\mathrm{MPa}\cdot 10^{25}\mathrm{m}^{-2})^{-1}$	3.0×10^{-4}
SiC median strength (MPa)	834
Weibull modulus (SiC)	8.0

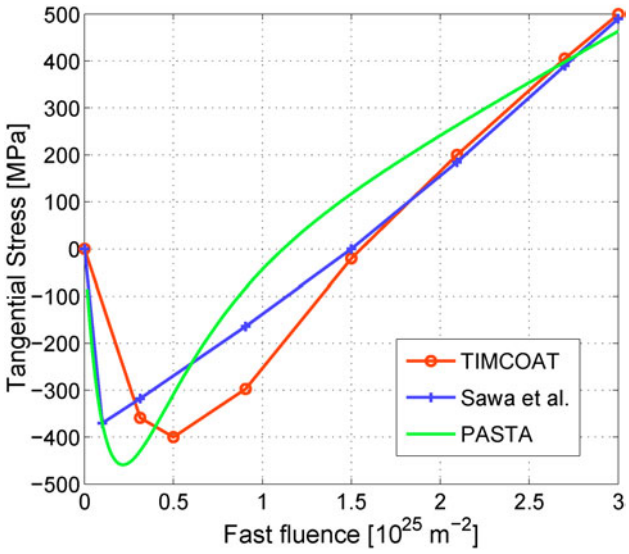

Fig. 13. Tangential stresses in the SiC layer calculated with PASTA and TIMCOAT[5] and by Sawa et al.[12] for the HTTR fuel during irradiation.

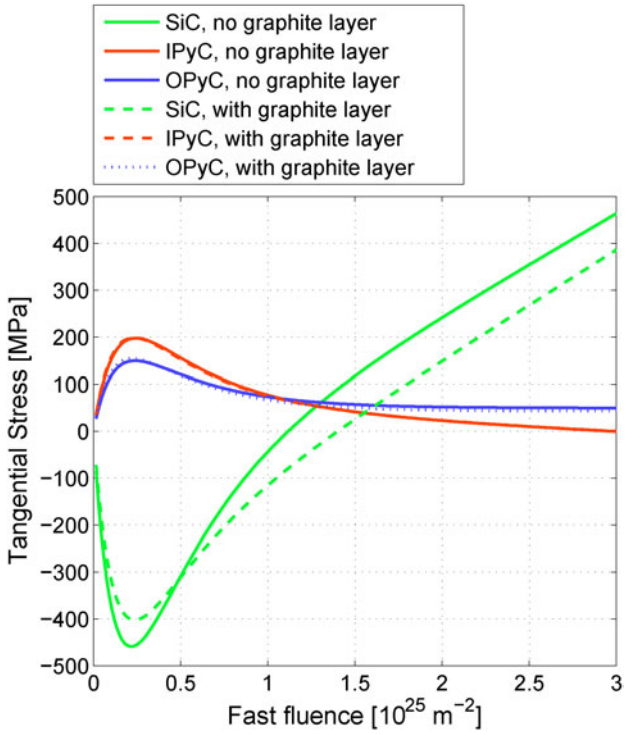

Fig. 14. Tangential stresses calculated with the PASTA code for the HTTR experiment with and without the presence of the graphite matrix.

beginning of irradiation, shrinkage of the PyC layers causes compressive (negative) tangential stresses in the SiC layer and positive tangential stresses in the PyC layers. This negative stress turns positive halfway through the irradiation by buildup of internal pressure caused by gaseous fission products and CO gas. The differences in the position and magnitude of the minimum SiC tangential stress are directly due to the different equations for the irradiation-induced dimensional change in the PyC layers introduced in the present model, by Sawa et al. and in the TIMCOAT code. Furthermore, the creep coefficients used by both authors for these layers was unknown and was set to 3.0×10^{-4} $(\text{MPa} \cdot 10^{25}\ \text{m}^{-2})^{-1}$ in the PASTA code. The stress calculated by Sawa et al. increases almost linearly after a decrease in stress at the beginning of irradiation. It is likely that a linear approximation was used to describe the stress during this irradiation interval.

The effects of graphite dimensional change are now analyzed by adding a graphite layer to the model that has a thickness of 400 μm. This thickness corresponds to a high packing fraction of particles in graphite, equivalent to the packing of 30 000 particles in a pebble, following the same calculation method for the thickness as in Sec. III.A. The fuel particles experience the same irradiation conditions as in the HTTR fuel experiment. The results for the coating stresses are presented in Fig. 14.

It is shown that the above-mentioned phenomena have an effect on the tangential SiC stress. The graphite compensates the shrinking of the PyC layers at the beginning of the irradiation because its tangential shrinking rate is smaller than that of the PyC layers, resulting in a reduced compressive stress on the SiC layer. When irradiation progresses, the isotropically shrinking matrix material offsets the stress induced by the radial swelling of the PyC layers. The particle is compressed by the matrix material, which reduces the tensile tangential stress in the SiC layer.

Finally, the failure probabilities of the SiC have been calculated by use of Eq. (38). It is found that the failure probability is 5.0×10^{-3} for the three-layer coated particle and 1.4×10^{-4} for the four-layer particle including dimensional change of the graphite matrix. The reduction in failure fraction results from a reduction in the tensile tangential stress of the SiC layer for the case with an additional graphite layer.

V.B. Stress Analysis of Particle Fuel in a 400-MW(thermal) HTR

As a second application, PASTA is used to calculate stresses in the fuel of a 400-MW(thermal) HTR similar to the Pebble Bed Modular Reactor (PBMR-400) design. Data concerning this reactor are taken from Ref. 33, and the general design characteristics are presented in Table III.

Simplifications were used in the neutronic model; i.e., the void regions, control rods, and reactor vessel were not modeled explicitly. By using the procedure described in Sec. IV, the neutron flux, burnup, power, and

TABLE III

Core Design Characteristics

Item	Value
Thermal reactor power (MW)	400
Helium inlet temperature (K)	773
Helium inlet temperature (K)	1 173
Height pebble bed (cm)	1 100
Radius inner reflector (cm)	100
Thickness pebble bed (cm)	85
Thickness outer reflector (cm)	90
Thickness top reflector (cm)	150
Thickness bottom reflector (cm)	150
Kernel diameter (μm)	500
Buffer thickness (μm)	95
IPyC thickness (μm)	40
SiC thickness (μm)	35
OPyC thickness (μm)	40
Uranium loading (g/pebble)	9
Enrichment (%)	9.6
Fuel particle per pebble	15 000
End-of-life burnup (GWd/t)	95

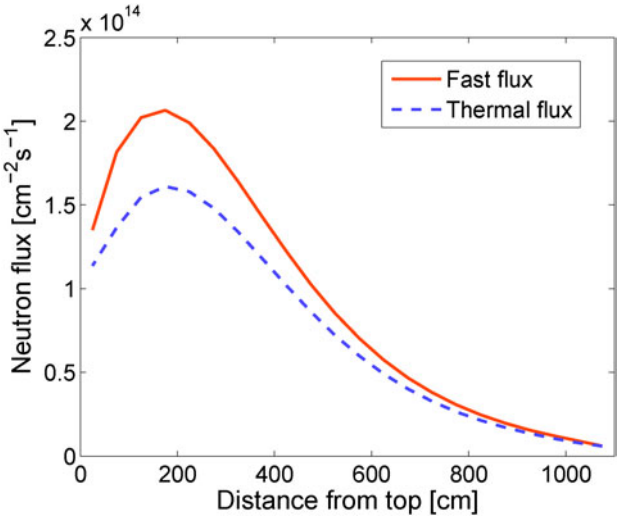

Fig. 15. Axial neutron flux profile in the pebble bed.

temperature profiles were calculated. Results are presented in Figs. 15 through 18. A coupled thermal-hydraulics–neutronics calculation was performed using temperature-dependent neutron cross sections and assuming a fixed reactor power, resulting in a k_{eff} of 1.0260. In the actual PBMR design, the presence of the control rods at the top of the side reflector results in a harder neutron

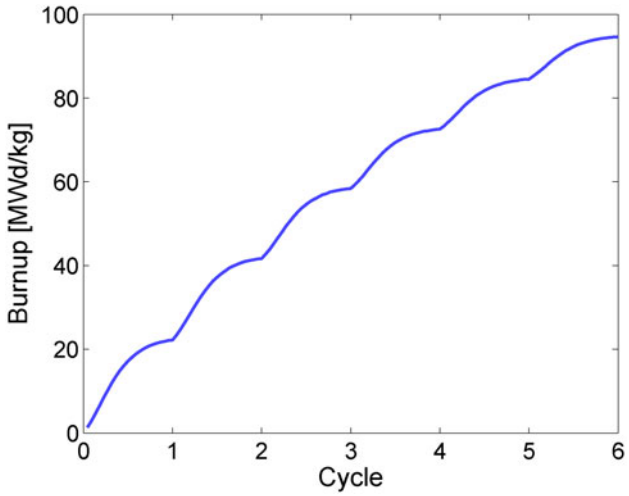

Fig. 16. Fuel burnup during irradiation (pebbles are cycled six times through the core).

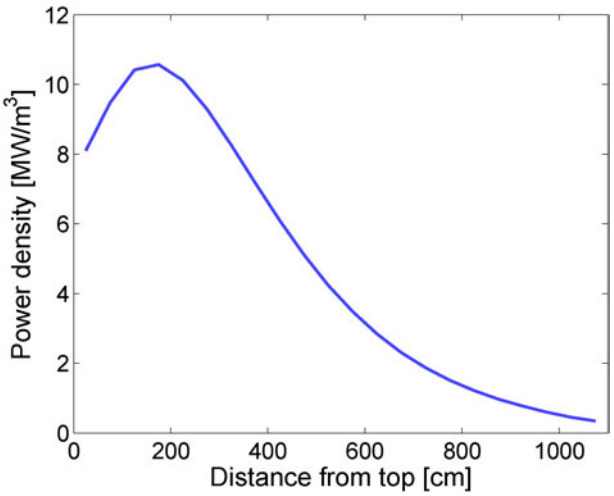

Fig. 17. Axial power profile in the pebble bed.

energy spectrum and a shift of the neutron flux peak away from the top (Fig. 15). In Fig. 16 the burnup level of the pebbles during irradiation is presented. After each cycle through the core, the pebbles reach considerably higher burnup, especially after the first cycle. The calculated power profile (Fig. 17) causes the maximum fuel temperature (Fig. 18) to rise quickly from top to bottom in the pebble bed before reaching a maximum value and decreasing slowly toward the bottom.

The pressure in the fuel particle and resulting tangential stress during irradiation are shown in Figs. 19 and 20, respectively. The pressure in the buffer layer increases during each cycle because of an increasing amount

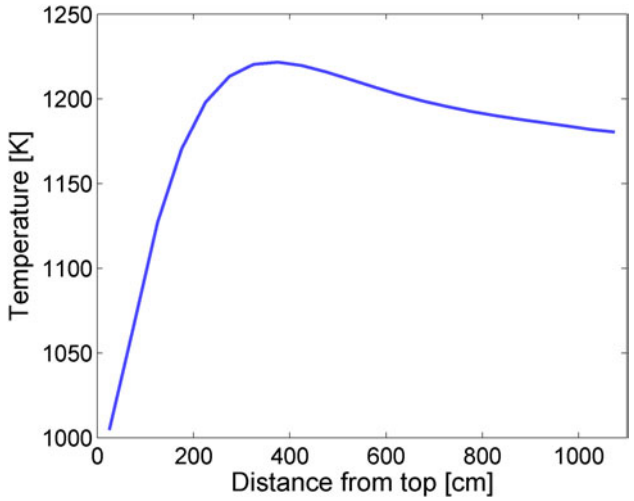

Fig. 18. Maximum fuel temperature profile in the pebble bed.

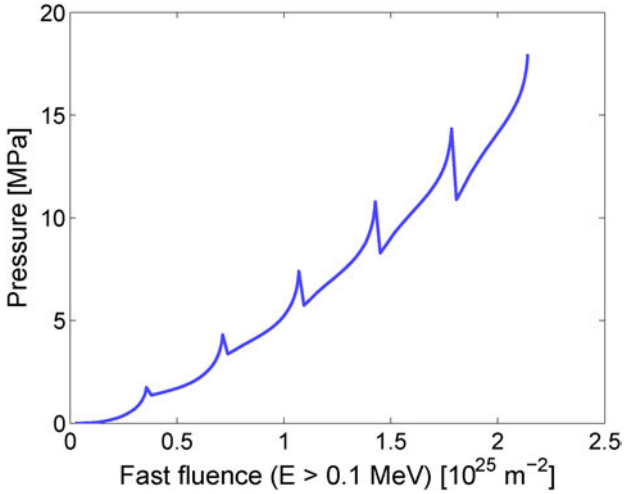

Fig. 19. Pressure in the buffer layer of a fuel particle in the center of a pebble during irradiation.

of gaseous fission products in the buffer and the high temperatures at the bottom region of the reactor core.

On one hand, the interparticle stress effects result in an additional radial tensile stress on the surface of each particle during irradiation. This causes a slight increase in the (tensile) tangential stress in the SiC layer at the end of the irradiation. However, the dimensional change of the graphite matrix causes a more important reduction in the tangential stress in the SiC layer (Fig. 20).

One can conclude from the results presented in Fig. 20 that for both cases (with or without graphite matrix stress effects), the SiC layer remains in compression. Therefore, the SiC layer does not fail directly from pressure buildup in the buffer layer. However, it has been shown that the SiC layer can fail indirectly after cracking of the PyC layers,[5,34] which results in a high local tensile stress around the crack tip.

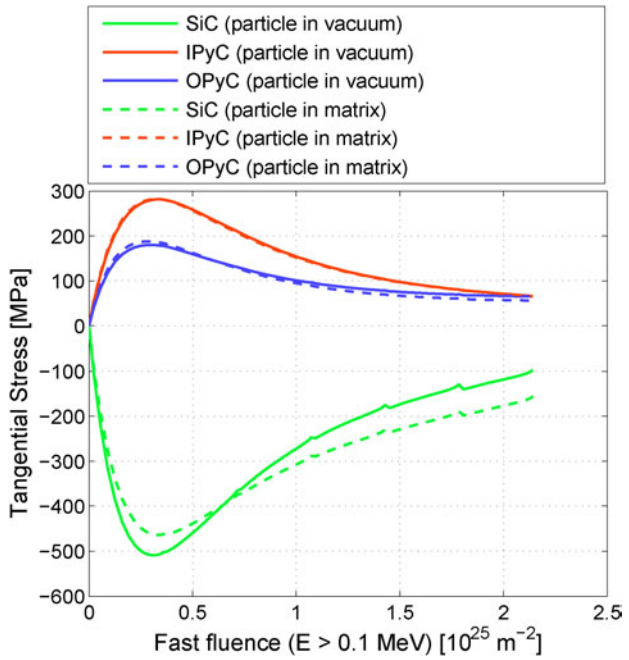

Fig. 20. Tangential stresses in particle coatings during irradiation for two cases: a single three-layer coated particle in vacuum (solid lines) and a three-layer coated particle in matrix material, which includes interparticle stress and graphite matrix dimensional change (dashed lines).

During accident situations the temperature in the reactor may increase, resulting in increased pressure in the buffer layer and possible tensile stress in the SiC layer. This leads to an increased failure probability of the SiC layer, especially at the end of the irradiation period. The presence of the graphite layer reduces this tensile stress, resulting in a lower failure probability of the SiC layer during the transient.

Figure 20 shows that the tangential stresses in the IPyC and the OPyC layers are almost unaffected by the presence of the graphite. Consequently, the failure probability of these layers by cracking of the pyrocarbon material is also unaffected.

VI. CONCLUSIONS

A stress analysis code was developed in order to analyze stress in fuel of HTR pebble bed designs. Existing analytical stress analysis models for coated particle fuel were expanded with an additional layer in order to

take into account stress effects due to dimensional change of the graphite matrix and neighboring particles. This analytical model allows for fast calculation of particle stresses and can therefore be easily applied in various fuel performance codes.

Shrinkage of the graphite matrix will cause an additional compressive stress on the particle during irradiation, which is usually beneficial for particle endurance. However, for certain types of graphite and temperature ranges, the shrinkage turns to swelling, which leads to an increase in particle failure at high irradiation dose. It is therefore important to have good data on the dimensional change and creep of the graphite matrix for analyzing stresses in coated particle fuel.

As a first approximation, the stresses coming from neighboring particles are modeled as a uniform stress on the outer surface of a given fuel particle. In reality the stress on the outer surface will likely be nonuniform. An investigation of the effect of the nonuniform stress field on the stresses in the particle using a finite element code is considered to be part of future work. Furthermore, the calculation procedure for interparticle stress effects might be improved by taking into account the nonlinear behavior of the creep in the summation of the individual stresses from neighboring particles. At high packing fractions, the neighboring particles can have a significant effect on the stress state of a given particle, which can result either in an increase or a decrease of the particle failure probability.

The stress analysis code was applied to an irradiation case of HTTR fuel. The tangential stress in the SiC layer calculated with PASTA and corresponding failure probability were comparable with results from Sawa et al.[12] for the three-layer model. A significant impact of the presence of the graphite matrix was encountered using the four-layer model. The failure probability of the SiC layer was found to be 5.0×10^{-3} for a particle in vacuum, while a value of 1.4×10^{-4} for a particle in the graphite matrix was found. This is caused by shrinkage of the graphite matrix, which results in a reduction of the tangential stress in the SiC layer.

In the application of PASTA to a 400-MW(thermal) HTR based on the PBMR-400 design, it was found that the SiC layer remains in compression during the entire irradiation period in the reactor. The presence of the graphite matrix results in an even higher compressive tangential stress in the SiC layer.

It is expected that shrinkage-induced cracking of the PyC layers can lead to possible failure of the SiC layer.[34] It is intended to incorporate this failure mechanism into the PASTA stress code.

For the dimensional change rates and creep coefficients of pyrolytic and matrix graphite, large differences can be found in the literature. For future validations it is important that the material properties that will be used in the model are applicable for the neutron flux and temperature range at which the experiment was conducted.

APPENDIX

COEFFICIENTS USED IN STRESS ANALYSIS EQUATIONS

$$K_1 = -\frac{2r^3 r_a^3(1-2\mu) + r_a^3 r_b^3(1+\mu)}{2Er^2(r_b^3 - r_a^3)} \quad , \tag{A.1}$$

$$K_2 = \frac{2r^3 r_b^3(1-2\mu) + r_a^3 r_b^3(1+\mu)}{2Er^2(r_b^3 - r_a^3)} \quad , \tag{A.2}$$

$$K_3 = -\frac{2r^3 r_a^3(1-2\nu) + r_a^3 r_b^3(1+\nu)}{2r^2(r_b^3 - r_a^3)} \quad , \tag{A.3}$$

$$K_4 = \frac{2r^3 r_b^3(1-2\nu) + r_a^3 r_b^3(1+\nu)}{2r^2(r_b^3 - r_a^3)} \quad , \tag{A.4}$$

$$K_5 = \frac{r_a^3 r_b^3 \ln \dfrac{r_a}{r_b}}{r^2(r_b^3 - r_a^3)} + \frac{r}{3} \quad , \tag{A.5}$$

$$K_6 = -\frac{r_a^3 r_b^3 \ln \dfrac{r_a}{r_b}}{r^2(r_b^3 - r_a^3)} + \frac{2r}{3} \quad , \tag{A.6}$$

and

$$K_7 = \frac{2(\nu - \mu)}{3E(\nu - 1)} \times \left[\frac{r_b^3(r^3 - r_a^3)\ln r_b - r_a^3(r^3 - r_b^3)\ln r_a}{r^2(r_b^3 - r_a^3)} - r \ln r \right] \tag{A.7}$$

NOMENCLATURE

a	= constant ($N \cdot m^4 \cdot K^{0.5} \cdot mol^{-2}$)
b	= constant ($m^3 \cdot mol^{-1}$)
C	= concentration of gaseous fission atoms ($atoms \cdot cm^{-3}$)
c	= irradiation-induced creep coefficient [$(MPa \cdot m^{-2})^{-1}$]
D	= diffusion coefficient ($cm^2 \cdot s^{-1}$)
E	= modulus of elasticity (MPa)
k	= thermal conductivity ($W \cdot m^{-1} \cdot K^{-1}$)
P	= pressure (Pa)
p	= radial stress acting on the inner surface of a radial layer (MPa)

Q = source of gaseous fission products (atom·$cm^{-3}\cdot s^{-1}$)

q = radial stress acting on the outer surface of a radial layer (MPa)

q''' = power density ($W\cdot m^{-3}$)

R = ideal gas constant ($J\cdot mol^{-1}\cdot K^{-1}$)

r = radial coordinate (μm)

$\dot{S}$ = dimensional change rate [$(m^{-2})^{-1}$]

T = temperature (K)

$\dot{T}$ = temperature change rate [$K\cdot(m^{-2})^{-1}$]

t = neutron fluence $E > 0.1$ MeV (m^{-2})

u = radial displacement (μm)

V_m = volume (molar) ($m^3\cdot mol^{-1}$)

Greek

α = thermal expansion coefficient (K^{-1})

ΔT = Temperature difference (K)

ε = strain ($\mu m/\mu m$)

μ = Poisson's ratio

ν = Poisson's ratio of creep

σ = stress (MPa)

Subscripts

a = inner surface of layer

b = outer surface of layer

f = fuel

g = graphite

gap = gap between buffer and IPyC layer

I = IPyC layer

$kern$ = fuel kernel

med = median

O = OPyC layer

peb = pebble

r = radial

S = SiC layer

$surface$ = surface of the pebble

t = tangential

X = graphite matrix layer

ACKNOWLEDGMENTS

This paper was written after an internship of B. Boer at the Idaho National Laboratory (INL) in the summer of 2006. The first author would like to thank A. M. Ougouag, G. K. Miller, and other colleagues at INL for their support during this internship.

REFERENCES

1. K. KUGELER and R. SCHULTEN, *Hochtemperatur-reaktortechnik*, Springer, Berlin (1989).

2. J. W. PRADOS and J. L. SCOTT, "Mathematical Model for Predicting Coated-Particle Behavior," *Nucl. Appl.*, **2**, 402 (Oct. 1966).

3. G. K. MILLER and R. G. BENNETT, "Analytical Solutions for Stresses in TRISO-Coated Particles," *J. Nucl. Mater.*, **206**, 35 (1993).

4. "Current Status and Future Development of Modular High Temperature Gas Cooled Reactor Technology," TECDOC 1198, International Atomic Energy Agency (Feb. 2001).

5. J. WANG, R. G. BALLINGER, and H. J. MACLEAN, "TIMCOAT: An Integrated Fuel Performance Model for Coated Particle Fuel," *Nucl. Technol.*, **148**, 68 (2004).

6. I-NERI, "Development for Improved Models and Designs for Coated Particle Gas Reactor Fuels," INEEL/EXT-05-02615, Idaho National Laboratory (2004).

7. B. LIU, T. LIANG, and C. TANG, "A Review of TRISO-Coated Particle Nuclear Fuel Performance Models," *Rare Metals*, **25**, *6*, 337 (Oct. 2006).

8. T. X. LIANG, H. S. ZHAO, C. H. TANG, and K. VERFONDERN, "Irradiation Performance and Modeling of the HTR-10 Coated Fuel Particles," *Nucl. Eng. Des.*, **236**, 1922 (2006).

9. M. PHELIP, F. MICHEL, M. PELLETIER, G. DEGENEVE, and P. GUILLERMIER, "The ATLAS HTR Fuel Simulation Code. Objectives, Description and First Results," *Proc. Int. Topl. Mtg. High Temperature Reactor Technology*, Beijing China, September 2004.

10. "A Technology Roadmap for Generation IV Nuclear Energy Systems," U.S. DOE Nuclear Energy Research Advisory Committee and the Generation IV International Forum (2002).

11. A. M. OUGOUAG, J. L. KLOOSTERMAN, W. F. G. VAN ROOIJEN, H. D. GOUGAR, and W. K. TERRY, "Investigation of the Bounds on the Particle Packing in Pebble-Bed High Temperature Reactors," *Nucl. Eng. Des.*, **236**, 669 (2006).

12. K. SAWA, S. SHIOZAWA, K. MINATO, and K. FUKUDA, "Development of a Coated Fuel Particle Failure Model Under High Burnup Irradiation," *J. Nucl. Sci. Technol.*, **33**, *9*, 712 (1996).

13. G. K. MILLER, "Stresses in a Spherical Pressure Vessel Undergoing Creep and Dimensional Changes," *Int. J. Solids and Structures*, **32**, *14*, 2077 (1995).

14. G. K. MILLER, "Considerations of Irradiation-Induced Transient Creep in Fuel Particle Modeling," *J. Nucl. Sci. Technol.*, **32**, *10*, 989 (Oct. 1995).

15. S. P. TIMOSHENKO and J. N. GOODIER, *Theory of Elasticity*, 3rd ed., McGraw-Hill, New York (1970).

16. G. K. MILLER, "Updated Solutions for Stresses and Displacements in TRISO-Coated Fuel Particles," Engineering Design File (EDF)-7042, Idaho National Laboratory (2006).

17. W. E. BOYCE and R. C. DiPRIMA, *Elementary Differential Equations and Boundary Value Problems*, 6th ed., John Wiley & Sons, New York (1996).

18. R. GONTARD and H. NABIELEK, "Performance Evaluation of Modern HTR TRISO Fuels," HTA-IB-05/90, Forschungszentrum Jülich (July 1990).

19. B. J. MARSDEN, "Irradiation Damage in Graphite," p. 17, IAEA-TECDOC-901 XA9642900, International Atomic Energy Agency (1995).

20. T. OKU, M. ETO, and S. ISHIYAMA, "Irradiation Properties and Strength of a Fine-Grained Isotropic Graphite," *J. Nucl. Mater.*, **172**, 77 (1990).

21. T. OKU and M. ISHIHARA, "Lifetime Evaluation of Graphite Components for HTGRs," *Nucl. Eng. Des.*, **227**, 209 (2004).

22. W. B. BICKFORD, *Advanced Mechanics of Materials*, Addison Wesley Longman (1998).

23. P. MKHABELA, J. HAN, B. TYOBEKA, K. IVANOV, F. REITSMA, and E. SARTORI, "Summary of Comparison and Analysis of Results from Exercises 1 & 2 of the OECD PBMR Coupled Neutronics/Thermal Hydraulics Transient Benchmark," *Proc. PHYSOR-2006*, Vancouver, British Columbia, Canada, September 10–14, 2006, American Nuclear Society (2006) (CD-ROM).

24. S. STRUTH, "Thermix-Direkt: Ein Rechenprogramm zur instationären zweidimensionalen Simulation thermohydraulischer Transienten," Forschungszentrum Jülich (1995).

25. B. BOER, J. L. KLOOSTERMAN, and A. M. OUGOUAG, "Optimization of HTR Fuel to Reduce Fuel Particle Failure," *Proc. PHYSOR-2006*, Vancouver, British Columbia, Canada, September 10–14, 2006, American Nuclear Society (2006) (CD-ROM).

26. "SCALE-5. Modular Code System for Performing Standardized Computer Analysis for Licensing Evaluations," Oak Ridge National Laboratory (2005).

27. E. E. BENDE, A. H. HOGENBIRK, J. L. KLOOSTERMAN, and H. VAN DAM, "Analytical Calculation of the Average Dancoff Factor for a Fuel Kernel in a Pebble Bed High-Temperature Reactor," *Nucl. Sci. Eng.*, **133**, *2*, 147 (1999).

28. D. OLANDER, *Fundamental Aspects of Nuclear Reactor Fuel Elements*, Technical Information Center, U.S. Energy Research and Development Administration (1976).

29. H. NABIELEK, K. VERFONDERN, and H. WERNER, "Can We Predict Coated Particle Failure? A Conversation on CONVOL, PANAMA and Other Codes," *Proc. Technical Mtg. Current Status and Future Prospects of Gas Cooled Reactor Fuels*, Vienna, June 2004.

30. E. PROKSCH, A. STRIGL, and H. NABIELEK, "Production of Carbon Monoxide During Burn-Up of UO_2 Kerneled HTR Fuel Particles," *J. Nucl. Mater.*, **107**, 28 (1982).

31. J. M. SMITH, H. V. VAN NESS, and M. M. ABOTT, *Introduction to Chemical Engineering Thermodynamics*, McGraw-Hill, New York (2001).

32. D. GROSS and T. SEELIG, *Fracture Mechanics*, Springer, Berlin (2006).

33. OECD, "PBMR Coupled Neutronics/Thermal Hydraulics Transient Benchmark—The PBMR-400 Core Design—Benchmark Description," Technical Report Draft-V03, Nuclear Energy Agency (Sep. 2005).

34. G. K. MILLER, D. A. PETTI, D. J. VARACALLE, and J. T. MAKI, "Consideration of the Effects on Fuel Particle Behavior from Shrinkage Cracks in the Inner Pyrocarbon Layer," *J. Nucl. Mater.*, **295**, 205 (Mar. 2001).